

Implications of statistics of near-range Doppler velocity observed with the Syowa East HF radar

Tadahiko Ogawa¹, Nozomu Nishitani¹, Natsuo Sato²,
Hisao Yamagishi² and Akira Sessai Yukimatu²

¹ *Solar-Terrestrial Environment Laboratory, Nagoya University, Honohara, Toyokawa 442-8507*

² *National Institute of Polar Research, Kaga 1-chome, Itabashi-ku, Tokyo 173-8515*

Abstract: A large data-set of line-of-sight Doppler velocity obtained with the Antarctic Syowa East HF radar from February to December 1997 is analyzed to discuss the statistical characteristics of Doppler velocity (V_D) at ranges of 180–1200 km and their implications. Syowa Station K -indices during the observation period were between 0 and 7 with a maximum occurrence at $K=1$. On average V_D has a minimum of about 100 m/s at 180–225 km ranges. With increasing range it increases monotonically to attain a maximum of 300–350 m/s at 400–500 km, decreases gradually to reach 250–300 m/s at about 700 km, and again increases slowly at farther ranges. These values of V_D and the range vary depending on both local time and radar beam direction. In the light of recent knowledge of plasma instabilities in the ionosphere we suggest that such range profile of V_D is mainly caused by the combined effects of altitude-dependent phase velocities of ionospheric plasma waves, HF wave refraction due to enhanced E region electron density, and latitude-dependent electric field. We infer that the low V_D (~ 100 m/s) at ranges of 180–225 km may originate in part from neutral winds and/or turbulence of the neutral atmosphere.

1. Introduction

The Syowa East HF radar located at Syowa Station, Antarctica (69.0°S , 39.6°E ; magnetic latitude 66.2°S ; L -value=6.1) is one of the Super Dual Auroral Radar Network (SuperDARN) coherent HF radars (Greenwald *et al.*, 1995). This radar can detect HF echoes backscattered at slant ranges from 180 to 3000 km (or more), that is, at altitudes including the ionospheric D , E , and F regions. HF waves are easily refracted in the E and F regions during propagation. The SuperDARN radars rely on the F region refraction to probe the F region at distant ranges. Before the advent of two SuperDARN HF radars (Syowa South and Syowa East) at Syowa Station, only a coherent VHF (50 MHz) radar had been operated to study phenomena associated with the auroral electrojets (Ogawa, 1996). VHF waves do not suffer appreciable refraction due to the ionospheric plasma. VHF radars at auroral latitudes can therefore probe only the D and E regions. E region echoes observed with the Syowa HF radars have been case-studied by Koustov *et al.* (2001) and Makarevitch *et al.* (2001) who used simultaneous 50 MHz radar echo data. They compared Doppler velocity and echo power from the HF radars and those from the VHF radar to discuss the similarity and dissimilarity between both radar results. One of their findings was that the effect of HF

wave refraction must be considered in explaining the HF data.

When HF backscatter is caused by geomagnetically field-aligned plasma irregularities, we may simply expect that echoes at near and distant ranges originate in the *D* and *E* regions and the *F* region, respectively, and that Doppler velocities detected with a radar are related to ionospheric electric fields. The actual situation, however, is not so simple as we expect since HF waves are usually refracted in the ionosphere. Because of this refraction, it is often difficult to determine true backscatter altitudes from observations. Moreover, near-range radar echoes from non-field-aligned irregularities (that is, echoes due to meteors and neutral atmosphere turbulence) may coexist with the ionospheric echoes originated from field-aligned irregularities.

This paper describes statistical results of the Doppler velocity observed at near ranges of 180–1200 km with the Syowa East radar. We do not intend to discuss detailed physical processes to explain the Doppler velocity characteristics. The physical features of *E* region HF radar echoes have been presented by, for example, Hanuise *et al.* (1991), Milan *et al.* (1997), Milan and Lester (1998), Koustov *et al.* (2001), and Makarevitch *et al.* (2001). In this paper we first introduce plasma instabilities in the *E* and *F* regions that can produce field-aligned electron density irregularities responsible for an HF wave backscatter. Then, range profiles of the Doppler velocity averaged over the period from February 1 to December 31, 1997 are presented to discuss their implications. Finally, we consider possible sources of the backscatter other than field-aligned irregularities. We suggest that low Doppler velocities (≤ 100 m/s) related to these sources may contribute in part to the velocity profiles at range less than 600 km.

2. Plasma instability

2.1. *E* region

Decameter-scale field-aligned irregularities in the ionosphere are produced through plasma instabilities. The two-stream (Farley-Buneman) and gradient-drift instabilities are important in the *E* region. Previous rocket measurements at Syowa Station showed that 5–200 m scale irregularities with relative amplitudes of 10% or less appear at altitudes of 90–120 km under various ionospheric conditions (Ogawa *et al.*, 1976). These irregularities are believed to have been excited through these instabilities. See a review paper by Haldoupis (1989) for the relationship between radio aurora and the *E* region plasma instabilities. The phase velocity (V_{ph}) and growth rate (Γ) derived from a linear dispersion relation including both instability processes are given by (e.g., Fejer *et al.*, 1984)

$$V_{ph} \equiv \frac{\omega_r}{k} = \frac{V_d \cos \theta}{1 + \Psi}, \quad (1)$$

$$\Gamma = \frac{\Psi}{1 + \Psi} \left(\frac{\omega_r^2 - k^2 C_s^2}{v_i} + \frac{\Omega_e}{v_e} \frac{\omega_r}{Lk} \right), \quad (2)$$

where

$$\Psi = \frac{v_e v_i}{\Omega_e \Omega_i} \left[\frac{k_{\perp}^2}{k^2} + \left(\frac{\Omega_e^2}{v_e^2} \right) \frac{k_{\parallel}^2}{k^2} \right] \equiv \Psi_0 \left[\cos^2 \alpha + \left(\frac{\Omega_e^2}{v_e^2} \right) \sin^2 \alpha \right]. \quad (3)$$

θ : Angle between radar wave vector (\mathbf{k}) and relative plasma drift velocity vector ($\mathbf{V}_d = \mathbf{V}_e - \mathbf{V}_i$),

\mathbf{B}_0 : Geomagnetic field vector,

ω_r : Wave frequency,

k : Wavenumber ($k^2 = k_{\parallel}^2 + k_{\perp}^2$),

k_{\parallel} : Wavenumber component parallel to \mathbf{B}_0 ,

k_{\perp} : Wavenumber component perpendicular to \mathbf{B}_0 ,

α : Aspect angle (that is, angle between \mathbf{k} and \mathbf{k}_{\perp}),

C_s : Local ion acoustic velocity,

ν_e (ν_i): Electron (ion)-neutral collision frequency,

Ω_e (Ω_i): Electron (ion) cyclotron frequency,

$\Psi_0 = \nu_e \nu_i / \Omega_e \Omega_i$,

L : Scale length of electron density gradient.

Below 115 km altitude, \mathbf{V}_d is almost equal to the electron drift velocity $\mathbf{V}_e (= \mathbf{E} \times \mathbf{B}_0 / B_0^2)$ where \mathbf{E} is the electric field vector. The first term in eq. (2) implies that when V_{ph} exceeds C_s , the stream-instability operates to produce type-1 irregularities. In the auroral E region the threshold of E is around 20 mV/m ($V_d = 400$ m/s). The gradient-drift instability (second term) to generate type-2 irregularities is excited whenever \mathbf{E} and ∇N_e (electron density gradient) have the same sign. V_{ph} , that is observed with a radar as Doppler velocity, is determined by three factors, V_d , θ , and Ψ . Ψ_0 included in Ψ increases rapidly with decreasing altitude; 0.01 at 108 km, 0.1 at 100 km, 1.0 at 93 km, and 10 at 87 km (Schlegel and Gurevich, 1997). V_d decreases above 115 km because \mathbf{V}_e approaches \mathbf{V}_i . Thus, V_{ph} is close to the $\mathbf{E} \times \mathbf{B}_0$ drift multiplied by $\cos \theta$ only at altitudes of 100–115 km, which means that in principle, we can know E from a Doppler measurement. However, Doppler velocities of the type-1 irregularities are usually near local C_s through non-linear processes (that is, V_{ph} saturates at C_s): therefore, we are unable to estimate E from the type-1 Doppler velocity. Another factor α (aspect angle) in eq. (3) also contribute to an increase in Ψ (that is, a decrease in V_{ph}). Radar echo power usually decreases very rapidly with increasing α , so that we can expect that the strongest echoes return from a point where $\mathbf{k} \perp \mathbf{B}_0$. Such effect is called the “geomagnetic aspect sensitivity”.

Dimant and Sudan (1995, 1997) have proposed a new plasma instability to produce field-aligned irregularities with wavelengths of several meters and longer at altitudes between 75 and 105 km (most probably below 90 km) where $\Psi_0 \gg 1$. This instability requires very strong E that exceeds 50 mV/m corresponding to an $\mathbf{E} \times \mathbf{B}_0$ drift velocity of 1000 m/s although V_{ph} would be less than 100 m/s because of very high Ψ_0 . Plasma waves that can be related to this instability have been observed by a rocket (Blix *et al.*, 1996) and an HF radar (Tsunoda *et al.*, 1997).

Field-aligned irregularities at altitudes between 90 and 100 km have been found by the 46.5 MHz middle and upper atmosphere (MU) radar of Kyoto University (Yamamoto *et al.*, 1991; Ogawa *et al.*, 1995). Although the echoes seem to have been caused by the gradient-drift instability, the echo power is extremely weak (≤ 10 dB) and the Doppler velocity is very low (≤ 50 m/s). Such echoes can only be observed with a very powerful radar such as the MU radar (peak power of 1 MW).

Recent theories tell that even if $E=0$ (no electric field), the gradient-drift instability can be excited by a neutral wind (\mathbf{U}_n) under the condition that $\mathbf{U}_n \times \mathbf{B}_0$ and ∇N_e have the same sign (Kagan and Kelley, 1998; Kagan *et al.*, 2000). Neutral winds can also drive a thermal instability (Kagan and Kelley, 2000). The applicability of these neutral wind-driven gradient-drift and thermal instabilities to the generation of decameter irregularities must be further checked on an experimental basis.

2.2. F region

Decameter-scale irregularities in the F region are also produced by plasma instabilities (e.g., Tsunoda, 1988). The two-stream instability is not operative in the F region. The gradient-drift instability, however, is still operative under the condition that $\mathbf{E} \times \mathbf{B}_0$ and ∇N_e have the same sign. In addition, field-aligned currents can invoke the current-convective instability. The growth rate including both instability processes is given by (Ossakow and Chaturvedi, 1979)

$$\Gamma = \frac{(n_0^{-1} dn_0/dy) [(v_i/\Omega_i) V_0 + (k_{\parallel}/k_x) V_{\parallel}]}{[(\Omega_i/v_i) + (\Omega_e/v_e)] (k_{\parallel}^2/k_x^2) + (\Omega_i/v_i)} = \Gamma_1 + \Gamma_2, \quad (4)$$

where

Γ_1 : Growth rate of the gradient-drift instability,

Γ_2 : Growth rate of the current-convective instability,

$V_{\parallel} = V_{i\parallel} - V_{e\parallel}$,

$V_{i\parallel}$: Ion drift velocity along \mathbf{B}_0 ,

$V_{e\parallel}$: Electron drift velocity along \mathbf{B}_0 ,

$V_0 = E/B_0$.

Equation (4) tells that Γ is independent of $|\mathbf{k}|$ and only dependent on the angle between \mathbf{k} and \mathbf{B}_0 . Unstable waves excited by the current-convective instability propagate nearly along x -axis under the conditions of \mathbf{E} along x -axis, ∇N_e along y -axis, and \mathbf{B}_0 along z -axis, under which the gradient-drift instability is stable (Γ_1 is negative). $\Gamma_2 = 0$ when $V_{\parallel} = 0$ (no field-aligned current): in this case, $\Gamma = \Gamma_1 \approx (n_0^{-1} dn_0/dy) V_0$ that gives the growth rate of the gradient-drift instability in the F region (note that Γ_1 is positive when \mathbf{E} is antiparallel to y -axis). Previous HF radar observations indicated that F region irregularities move at the drift speed of $\mathbf{E} \times \mathbf{B}_0 / B_0^2$ (Ruohoniemi *et al.*, 1987). This fact is not always valid in the E region as described above.

3. Observations

3.1. Syowa East radar

Figure 1 shows the field of view (FOV) of the Syowa East radar in geographic coordinates. The FOV is covered with 16 narrow beams (beam numbers 0, 1, 2, ..., 15; each beam width $\sim 3.5^\circ$) over an azimuth sector of 52° . The beam direction of beam 0 is almost perpendicular (80°) to the magnetic L -shells and that of beam 15 has an angle of 20° to them. The radar beam in the normal SuperDARN operation is sequentially scanned from beam 0 to beam 15 (16 azimuth bearings) with a step in azimuth of 3.3° , a scan repeat time of ~ 120 s, a range resolution of 45 km, and a peak

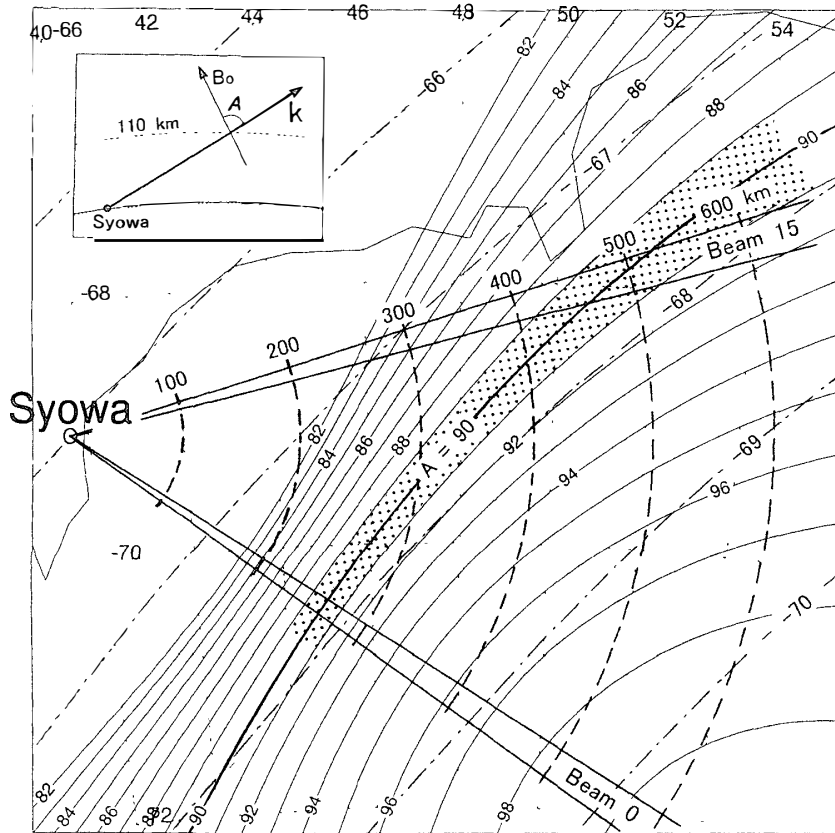


Fig. 1. Field of view of the Syowa East HF radar covered with 16 narrow beams (beam numbers 0, 1, 2, ..., 15) in geographic coordinates. Geomagnetic latitudes are shown by the dot-dashed curves. Ground ranges (100 km step) from Syowa Station are marked by the dashed curves. Contour lines of angle (A) between radar wave and the geomagnetic field vectors at an altitude of 110 km are shown by the solid curves.

power of around 10kW. The first range gate is set to 180km.

Coherent radar echoes are strongly backscattered from an area where the angle (“ A ” in Fig. 1) between the radar wave vector (\mathbf{k}) and the geomagnetic field vector (\mathbf{B}_0) is 89° – 91° (see Section 2). Such area at an altitude of 110 km is shaded in Fig. 1. The area is located at ground ranges of around 270 km on beam 0 and around 500 km on beam 15. Note that the aspect angle $\alpha \equiv 90^\circ - A$. Previous VHF (50 MHz) radar observations at Syowa Station indicated that echoes on a radar beam nearly perpendicular to the L -shells are strongest at a range of around 280 km (Ogawa and Igarashi, 1982; Ogawa *et al.*, 1989; Koustov *et al.*, 2001). Note that no radar wave refraction during propagation is assumed in the calculations. This assumption is almost valid for VHF waves.

The aspect angle distribution shown in Fig. 1 varies depending on altitude. Altitude and range distributions of α on beams 0 and 15 are plotted in Fig. 2 where the areas having α between -1° and $+1^\circ$ are shaded on the ray paths from Syowa. On beam 0 (Fig. 2a) the radar waves with elevation angles of 18° – 20° are backscattered from altitudes of 100–120 km at slant ranges of 250–300 km while on beam 15 (Fig. 2b), these values are 7° – 13° and 400–600 km. The path length crossing the E region altitude becomes longer with increasing beam number. It is clear that F region echoes can be

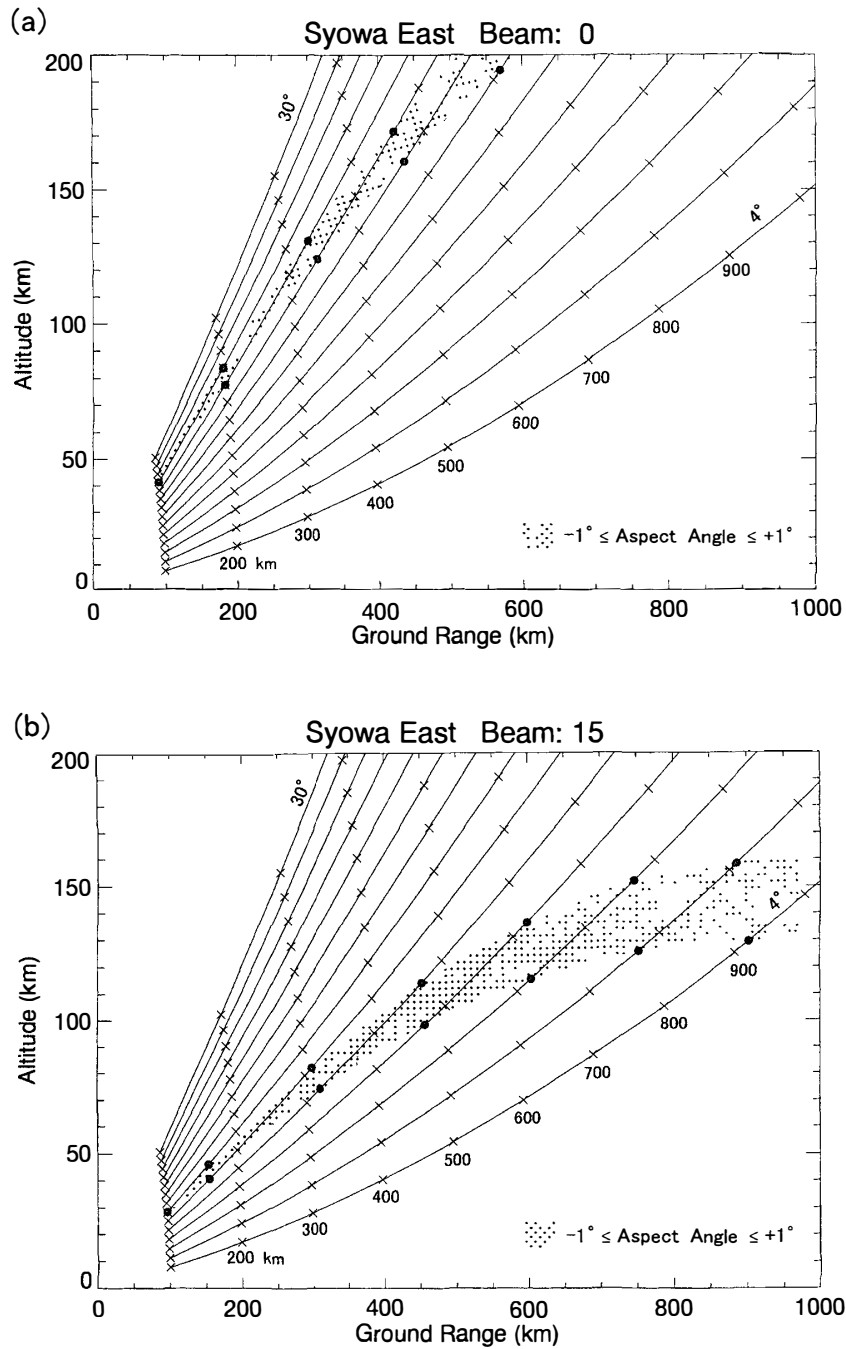


Fig. 2. Area (shaded) having aspect angles between -1° and $+1^\circ$ for ray paths with elevation angles of 4° – 30° (2° step) on (a) beam 0 and (b) beam 15 of the Syowa East radar. Slant ranges (100 km step) from Syowa Station are also indicated.

observed at distant slant ranges with lower elevation angles.

3.2. Example

Figure 3 displays examples of the near range echoes observed on beam 0 (Fig. 3a) and beam 13 (Fig. 3b) on July 15, 1997. Note that $UT \approx$ magnetic local time (MLT) at Syowa Station. The radar frequencies used are around 10 MHz. The top, middle,

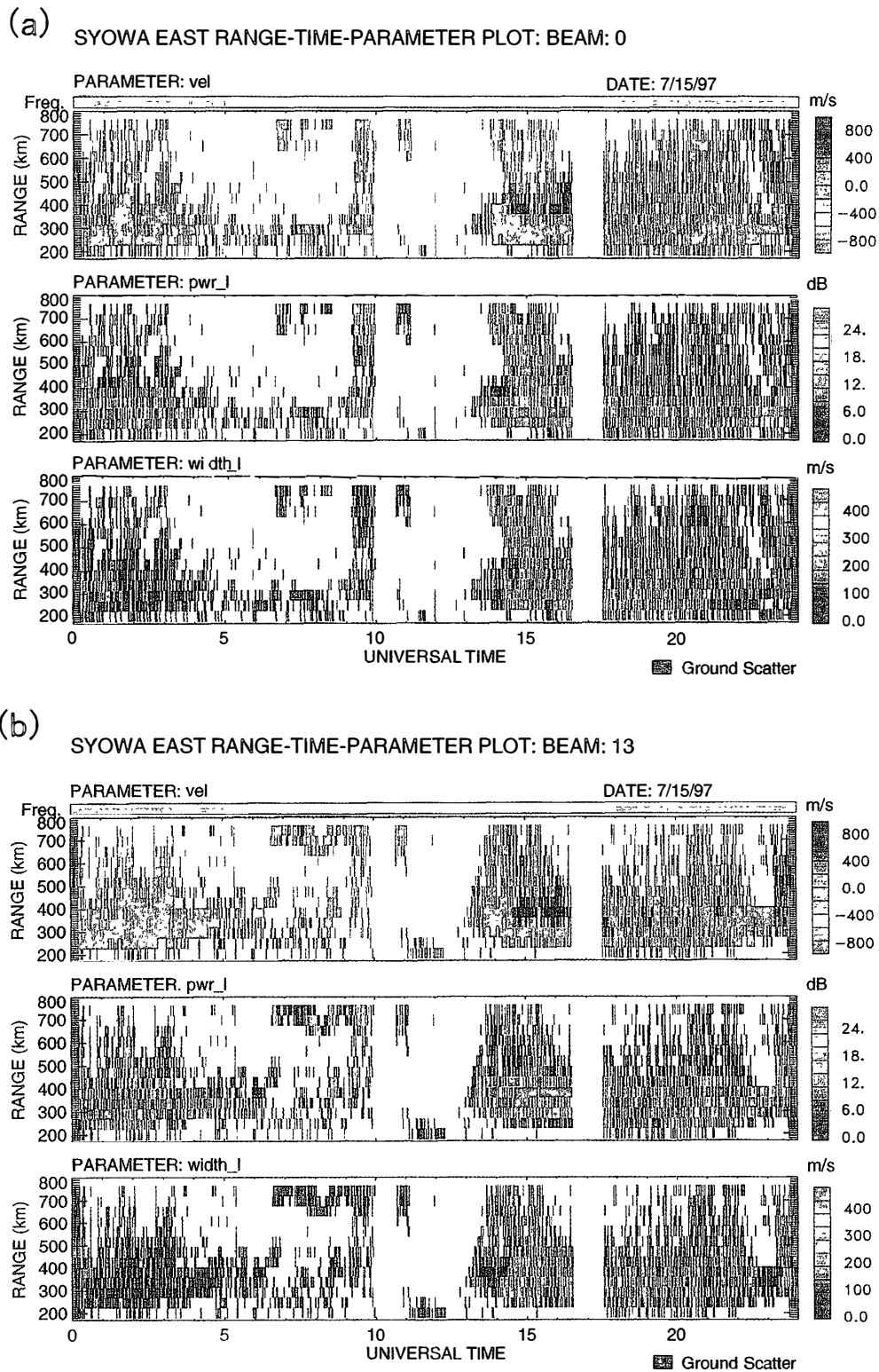


Fig. 3. Slant range-time plots of Doppler velocity (*vel*; positive toward the radar), echo power (*pwr*), and spectral width (*width*) on (a) beam 0 and (b) beam 13 observed with the Syowa East radar on July 15, 1997. The radar frequencies are around 10 MHz. Ground scatter echoes are indicated by gray color. Data are not plotted for the periods of no radar operation (1000–1040 and 1630–1730 UT).

and bottom panels in each figure show slant range-time plots of the Doppler velocity (vel), echo power (pwr), and spectral width (width), respectively. Plus (minus) sign of the Doppler velocity means motion toward (away from) the radar. The short-lived (≤ 120 s) and isolated echoes are due to meteors and partly due to radio interference from other sources. In Fig. 3a the echoes are intensified at 00–03 and 13–23 UT at ranges of 225–315 km where α 's are close to 0° at altitudes of 90–120 km (Fig. 2a). In Fig. 3b the echoes are strongest at the nearly same hours at ranges of 270–405 km where again α 's are close to 0° in the *E* region. These facts indicate that the radar wave refraction was not important on this date although the ionosphere was moderately disturbed as inferred from 3-hour *K*-indices at Syowa Station (2, 2, 1, 3, 3, 3, 4, 4).

The Doppler velocities in Fig. 3b are negative before about 15 UT and positive after that, which means that beam 13 detected eastward electron drifts (westward electrojet) before 15 UT and westward drifts (eastward electrojet) after 15 UT, being a reasonable result judging from the two-cell convection flows at auroral latitudes (e.g., Heppner and Maynard, 1987). Such behaviors are also discernible on beam 0 (Fig. 3a) that has an angle of 80° relative to the *L*-shells.

As can be seen in Fig. 3, the echo regions extend to ranges beyond 500 km. These echoes are believed to originate in the upper *E* and *F* regions. Notice the positive velocities at 21–24 UT on both beams that were probably caused by equatorward plasma flows near the Harang discontinuity before midnight. The strongly positive velocities (≥ 800 m/s) at ranges of 360–500 km during 14–16.5 UT on both beams might be due to strong westward and equatorward plasma flows that appeared locally in the eastward flow region.

3.3. *K*-index at Syowa Station

Occurrence, amplitude, and movement of the decameter-scale irregularities depend on geomagnetic (ionospheric) conditions; they are more intensified under more disturbed conditions. This is because the irregularity production, growth, and movement are strongly controlled by electric field, electron density gradient, and field-aligned currents (Section 2). As a measure of the ionospheric condition over Syowa Station, we use 3-hour *K*-index derived from a magnetogram at Syowa Station. *K*-indices for the period from February 1 to December 31, 1997 have been tabulated by Takeuchi *et al.* (1999). The relationship between *K*-index and amplitude of deviation of the geomagnetic field from a quiet level is as follows: $K=0$ for 0–25 nT, 1 for 25–50 nT, 2 for 50–100 nT, 3 for 100–200 nT, 4 for 200–350 nT, 5 for 350–600 nT, 6 for 600–1000, 7 for 1000–1660 nT, 8 for 1660–2500 nT, and 9 for ≥ 2500 nT.

Figure 4 gives histograms of the occurrence number of *K*-indices at eight 3-hour periods during 11 months. The histograms at 00–03 and 21–24 UT have a maximum at $K=3$ while the others except the 18–21 UT histogram show a peak at $K=1$, which means that the geomagnetic field at Syowa Station (66.2° S MLAT) was disturbed at around 18–03 UT when Syowa Station was below or close to the auroral electrojets. The occurrence number of *K*-indices during the whole period is displayed in Fig. 5 where the most probable *K* is 1. The occurrence number with $K=0$ and 1 (that is, quiet geomagnetic conditions) is 47.5% of the total occurrence number. *K*'s of 8 and 9 were not recorded through the period. Notice that HF radar echoes usually disap-

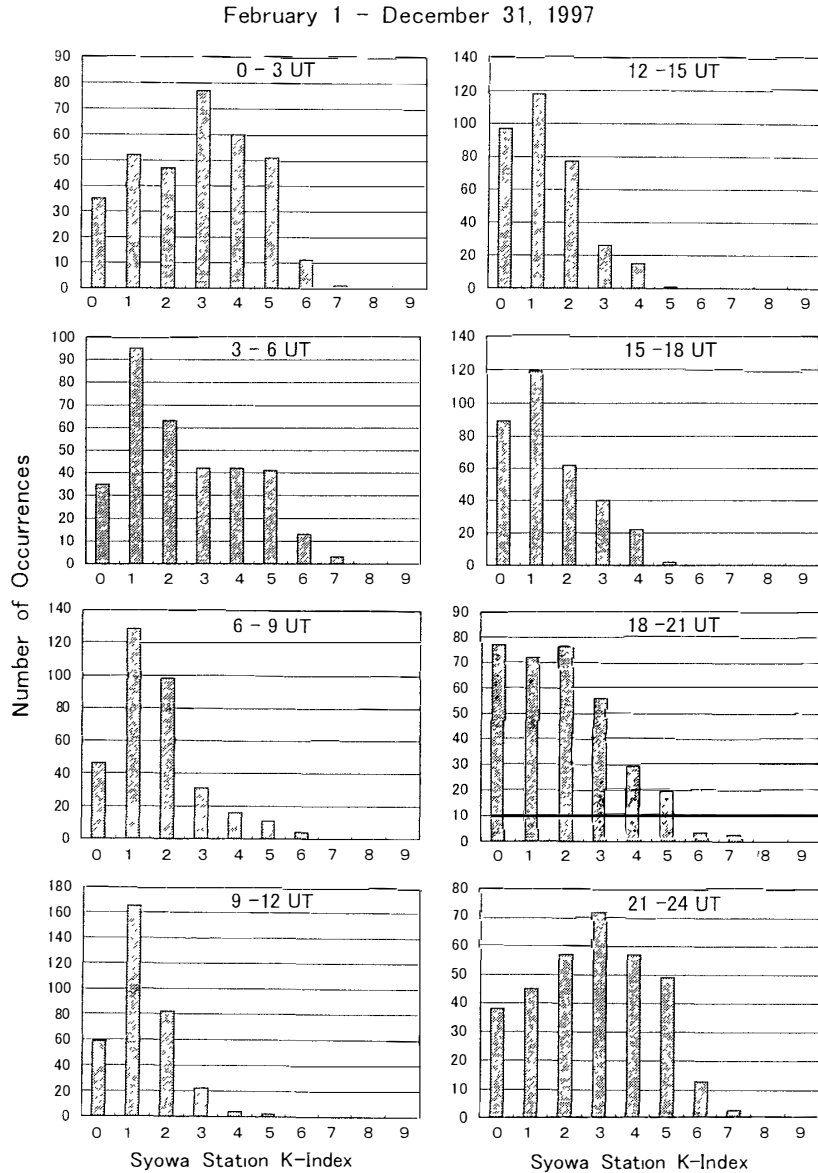


Fig. 4. Number of occurrences of Syowa Station K-indices at each 3-hour period during February 1–December 31, 1997.

pear during substorm conditions because of *D* region absorption.

4. Statistical results

4.1. Data selection

To derive range distributions of the line-of-sight Doppler velocity averaged over the whole period we first exclude anomalous echoes and ground scatter echoes from the original data base (note that each data point has time and range resolutions of 2 min and 45 km, respectively) using the following method (Fukumoto *et al.*, 1999, 2000):

1) Anomalous echoes satisfying at least one of the following criteria are eliminated: (1) an echo power of below 0 dB or above 30 dB, (2) a Doppler velocity beyond ± 1000 m/s, or (3) a spectral width beyond 1000 m/s.

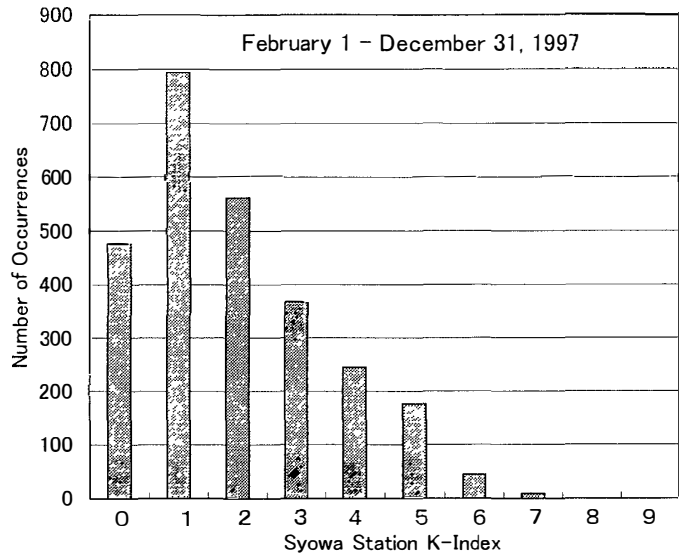


Fig. 5. Number of occurrences of Syowa Station K-indices during February 1–December 31, 1997.

2) Echoes with a Doppler velocity within ± 60 m/s as well as a spectral width less than 60 m/s are omitted as ground scatter echoes.

Moreover, to eliminate undesirable echoes due to meteor, noise, radio interference, and others, we use only data satisfying the following conditions at the same time:

3) Echoes detected at more than 3 consecutive radar range gates (≥ 90 km) and lasting for more than 2 min (usually for at least two radar scans).

4) Echoes with Doppler velocities that increase or decrease monotonically over 3 consecutive range gates or that exhibit a small difference ($\leq 33\%$) between adjacent range gates.

We believe that the above procedure for the data selection can eliminate non-ionospheric echoes from the original data base and may pick up only echoes due to ionospheric irregularities. Finally, we divide the selected Doppler velocities into two groups, plus-sign and minus-sign groups, according to velocity sign. This is because when data from two groups are mixed, data points are tremendously scattered. We presume that echoes with the plus-sign (minus-sign) Doppler velocities return mainly from the eastward (westward) electrojets. We then calculate mean value and standard deviation of the velocities for each group.

4.2. Range profile of Doppler velocity

a. Profile averaged over all hours

Figure 6 plots range profiles of the mean Doppler velocity and standard deviation on beam 0 (Fig. 6a) and beam 15 (Fig. 6b). In these plots all the data covering all hours from February 1 to December 31, 1997 are used. The number of total data points is 174977 and 101951 in Figs. 6a and 6b, respectively.

In Fig. 6a the mean velocity profile with positive sign is very similar to that with negative sign. The mean velocity is 100 m/s at 180 km (minimum range), 70 m/s (minimum velocity) at 225 km, 300 m/s (maximum velocity) at 405 km, and 200–250 m/s beyond 585 km. Figure 2a suggests that these ranges (180, 225, 405, and 585 km) correspond to altitudes of about 80, 90, 150, and 190 km, respectively, which means that the maximum velocity of 300 m/s appears at 150 km altitude in the F region. This

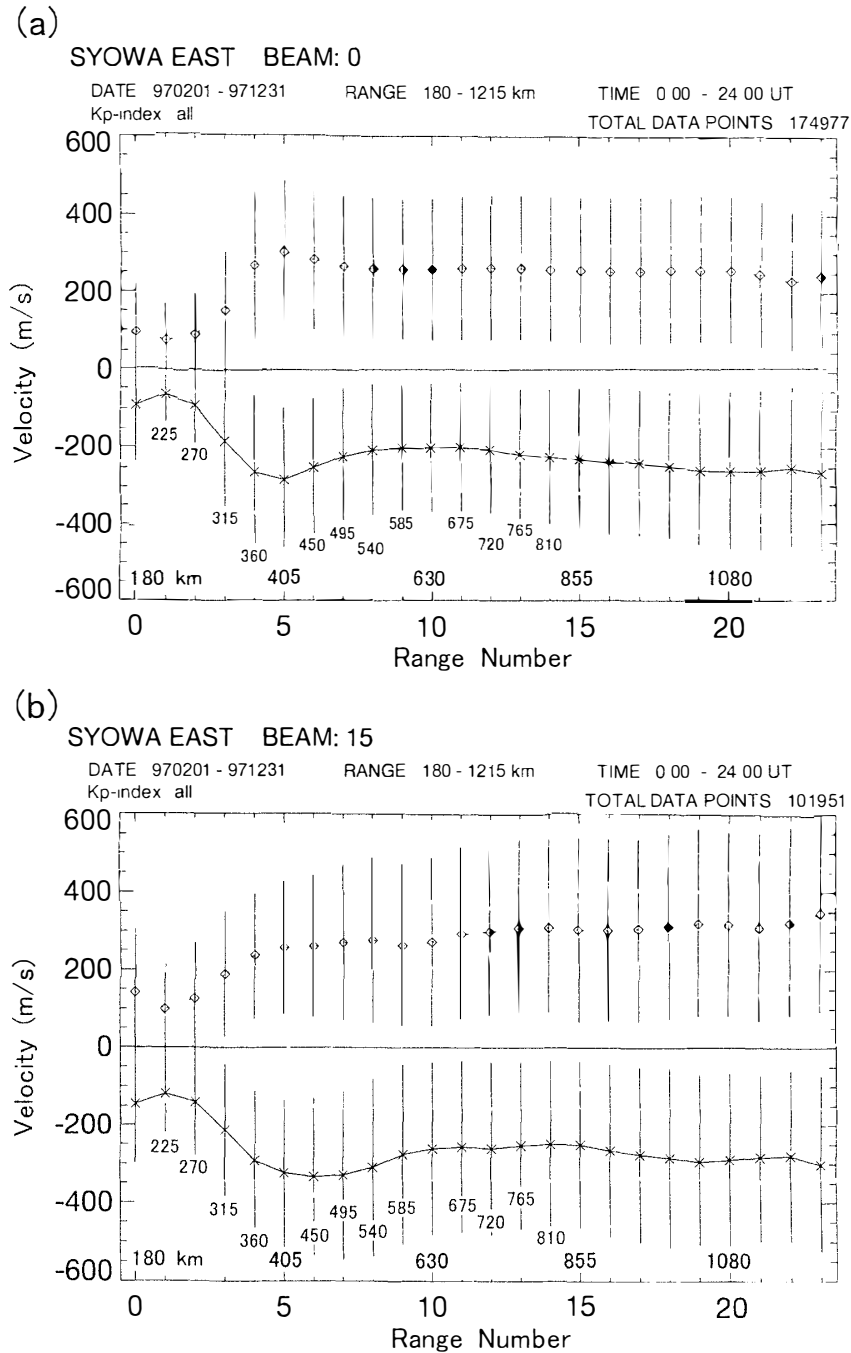


Fig. 6. Range profiles of Doppler velocity with positive (dotted line) and negative (solid line) sign, averaged over all hours during February 1–December 31, 1997, for (a) beam 0 and (b) beam 15 of the Syowa East radar. The vertical lines mean standard deviations. The total data points used for the analysis are (a) 174977 and (b) 101951

result is curious because as stated in Section 2, it is expected that the maximum phase velocities of plasma waves produced by the two-stream and/or gradient-drift instabilities should appear at around 110 km altitude corresponding to a slant range of 280 km (Fig. 2a). There are two possibilities to resolve this discrepancy. One possibility is that the radar echoes with the maximum velocity were backscattered at an altitude of 110 km

instead of 150 km: in this case the aspect angle at the 405 km range should be around 6° (Fig. 1). However, we cannot expect the radar echoes from a point with such a large aspect angle because of the aspect sensitivity. The other possibility is the ionospheric refraction of the HF radar waves. HF waves are easily refracted downward during oblique propagation due to electron density gradient of the bottomside of the E region (such effect is not considered in Figs. 1 and 2). Relying on this, our result can be explained in a way that the radar waves were actually backscattered at an altitude of about 110 km at a range of about 400 km where the aspect angle is close to zero.

General behavior of the mean velocity profile on beam 15 (Fig. 6b) is similar to Fig. 6a; 150 m/s at 180 km, 100 m/s (minimum velocity) at 225 km, 250–330 m/s (maximum velocity) at 450–540 km, and 270–300 m/s beyond 700 km. The ranges where the maximum velocity appears are located at altitudes of 100–120 km (Fig. 2b), which means that the radar wave refraction is not important.

To see a dependence of the Doppler velocity profile on beam number (*i.e.*, on the angle between the beam direction and *L*-shells), Fig. 7 plots range profiles on beams 0, 1, 7, 8, 14, and 15. The beam 0, 7, and 14 profiles are very similar to the beam 1, 8, and

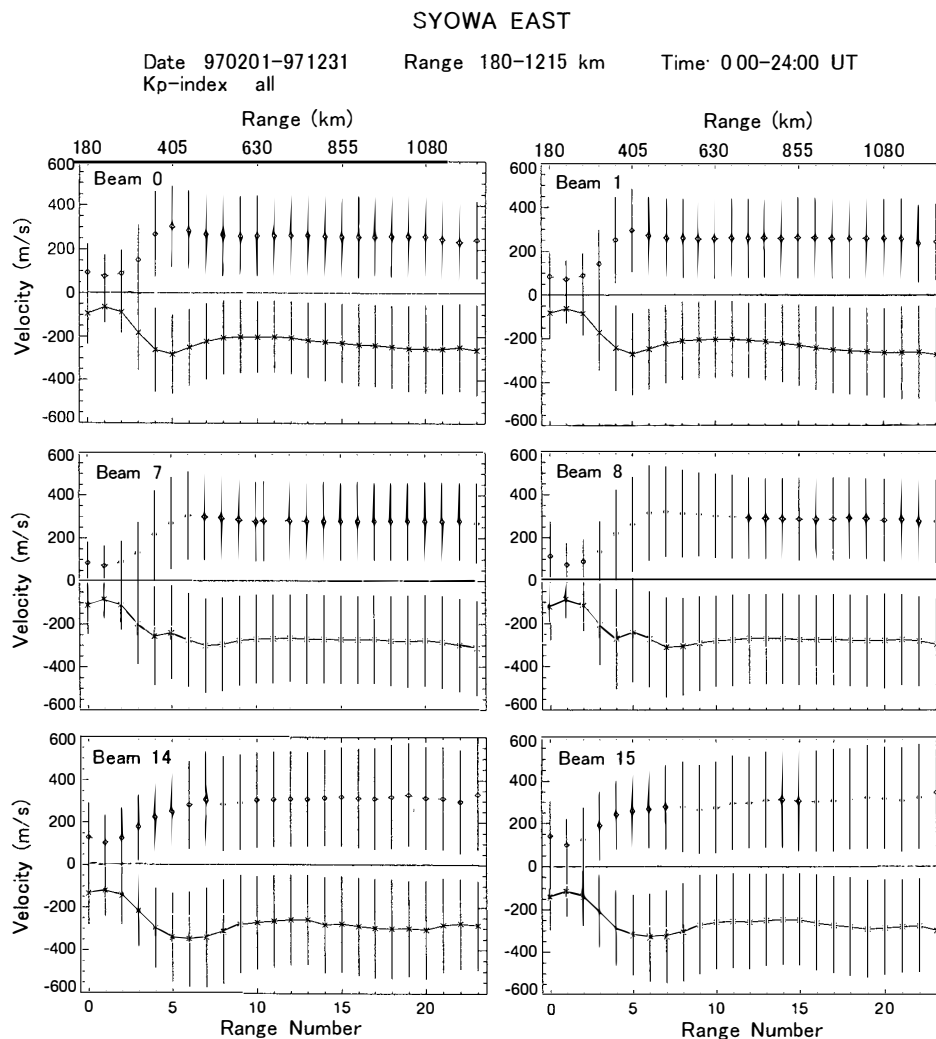


Fig. 7. Same as Fig. 6 but for beams 0, 1, 7, 8, 14, and 15.

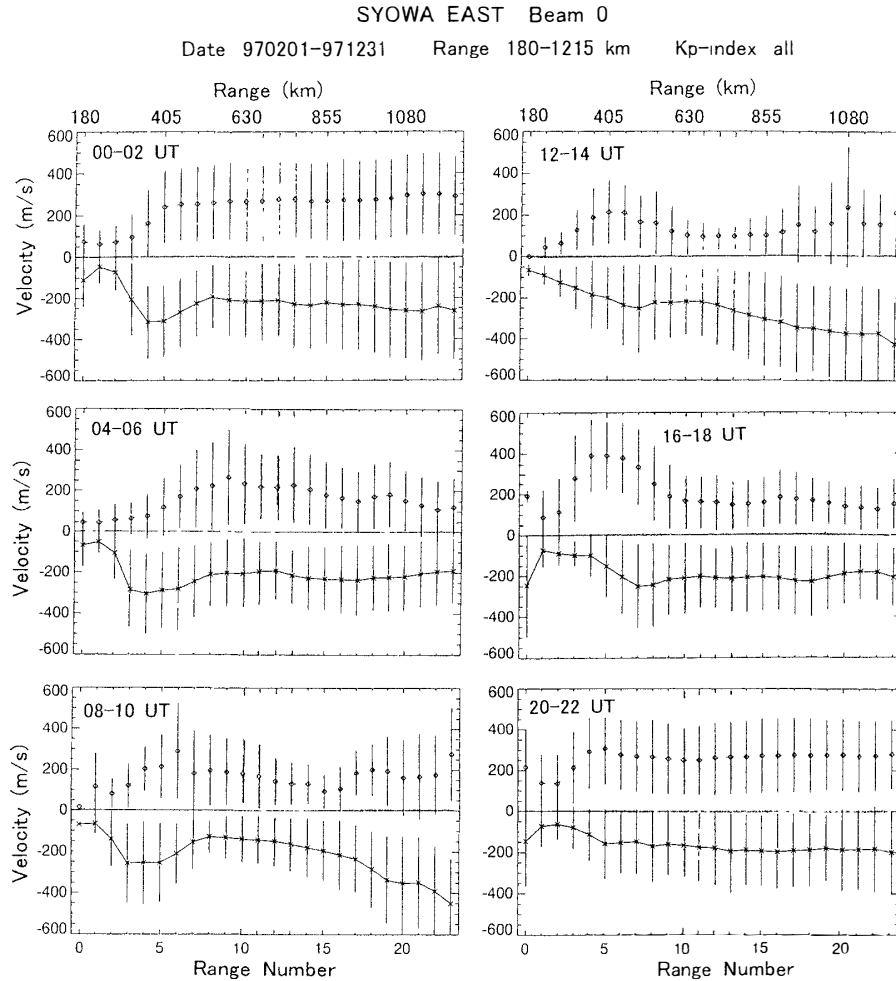


Fig. 8. Range profiles of Doppler velocity with positive (dotted line) and negative (solid line) sign, averaged over 2-hour period during February 1–December 31, 1997, for beam 0 of the Syowa East radar. The vertical lines mean standard deviations.

15 profiles, respectively. Moreover, the beam 7 and 8 profiles are similar to the beam 14 and 15 profiles. This fact suggests that the wave refraction is not important for beams 7–15 that have angles of 20° – 50° between the beam direction and L -shells.

b. Time dependence of profile

Range profiles on beam 0 averaged over two hours are shown in Fig. 8. The profile changes with time. For the profiles with positive velocity at 12–22 UT a velocity peak appears at a range of about ~ 400 km (range number 5) while for the negative velocity profiles at 00–10 UT the peak exists at ranges of about 360 km (range number 4). These positive and negative velocities in the afternoon and in the morning, respectively, are consistent with those from a model of the two-cell convection at a latitude of 67.5° (e.g., Heppner and Maynard, 1987) telling that the plasma drifts are toward west (east) in the afternoon (morning) cell that corresponds to the negative (positive) Doppler velocity for the Syowa East radar. None of the profiles show a velocity maximum at a range of about 280 km, again suggesting that the wave refraction is essential for beam 0.

Figure 9 shows range profiles on beam 15 averaged over two hours. Compared

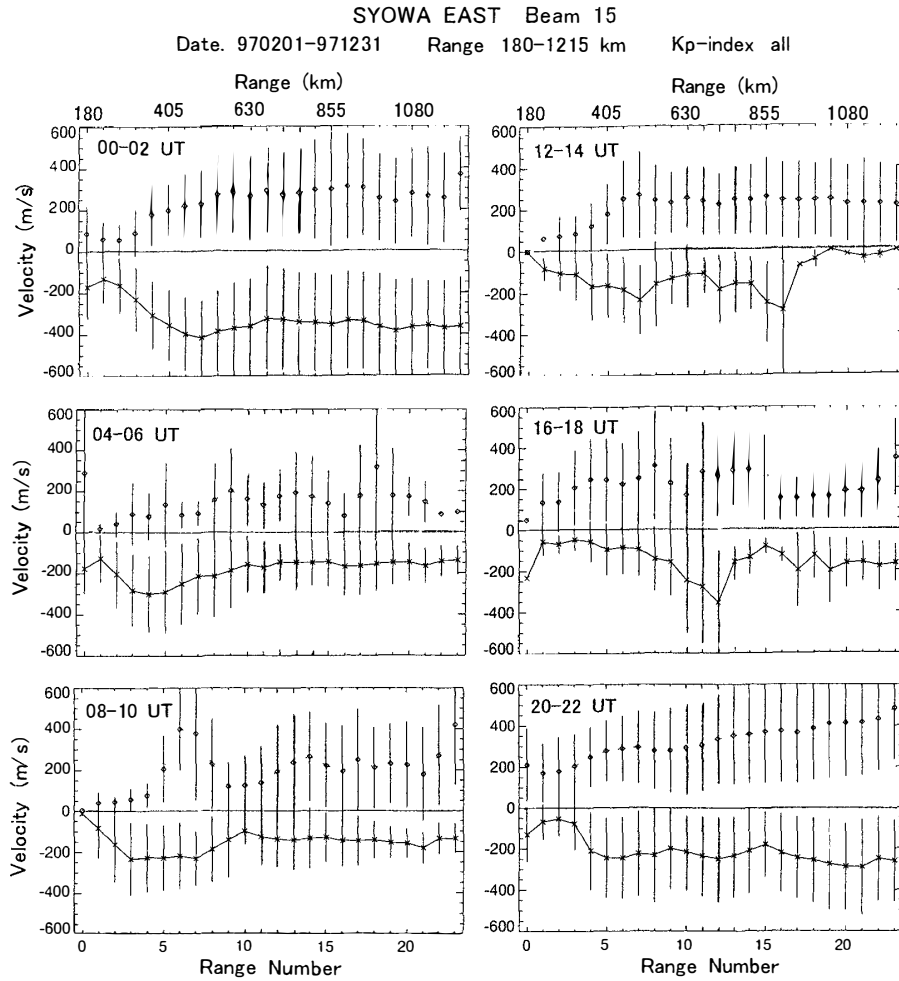


Fig. 9. Same as Fig. 8 but for beam 15.

with Fig. 8, temporal change of the profile is more variable. The largely undulated profiles are due to small data points. For the positive velocity profiles at 08-18 UT the velocity peaks occur at ranges of 450-500 km while for the negative velocity profiles at 20-10 UT they appear at ranges of 360-500 km. These positive and negative velocities are also consistent with those from the plasma flow model. Again, the wave refraction is not important for beam 15.

5. Discussion

5.1. Range variation of Doppler velocity

Range profiles of Doppler velocity (V_D) averaged over 11 months indicate that V_D is $\sim 70-150$ m/s at ranges of 180-225 km, ~ 300 m/s at 400-500 km, and 200-300 m/s at ranges beyond 600 km. These values depend on radar beam number and local time. Radar wave refraction is important only for beams 0 and 1 that are nearly perpendicular to the L -shells. Because of this effect, the maximum of V_D appears at around 360 km in the morning (00-10 UT) and around 400 km in the afternoon (12-22 UT). A difference of 40 km in range may simply suggest that the altitude where V_{ph} has a maximum

is lower in the morning than in the afternoon. If this were the case, Ψ in eq. (1) would have a morning/afternoon asymmetry. When this altitude (~ 110 km) is unchangeable with time, the difference in range can be explained in terms of enhanced E region electron density that strengthens the HF wave refraction. Hardy *et al.* (1985) found statistically that average energy of precipitating hot electrons (≥ 600 eV) is highest on the morningside of the auroral oval, suggesting that the E region electron density in the morning is higher than that in the evening. If this is the case, our result suggests that when the E region electron density is enhanced, then a ray path to reach 110 km altitude should have path length shorter by around 40 km, compared with the case with weak electron density enhancement. The enhanced density in the morning can be related to the lowering of the center of the westward electrojet in the morning as compared with the eastward electrojet in the afternoon (Kamide and Brekke, 1977). The importance of wave refraction for the SuperDARN radars has been pointed out by Villain *et al.* (1984), Uspensky *et al.* (1994), Milan and Lester (1998), Koustov *et al.* (2001), and Makarevitch *et al.* (2001). The statistical analysis presented in this paper confirms their results.

To investigate HF ray paths in the ionosphere we tried ray-tracings of 10 MHz under a Chapman-type electron density distribution with a plasma frequency of 5 MHz at an altitude of 250 km and a scale height of 50 km (Ogawa *et al.*, 1990). The results are shown in Fig. 10 for azimuths of 140° and 80° , that is, for beams 0 and 15, respectively. The positions where ray paths are nearly perpendicular (between 89° and 91°) to the geomagnetic field are indicated by the crosses. Figure 10a (beam 0) tells that the slant ranges for the E region echoes at altitudes of 100–120 km are 300–350 km and that the echoes at ranges beyond 350 km are backscattered from the upper E and F regions. Our observations indicate a maximum velocity of about 300 m/s at a range of 400 km that corresponds to altitudes of 150–200 km in Fig. 10a. To locate the observed maximum velocity at the 110 km altitude, we need the wave refraction due to an enhanced electron density in the E region that is not considered in the present ray-tracings (Villain *et al.*, 1984). Such enhancements are very possible under disturbed ionospheric conditions with $K \geq 2$ (e.g., Miyazaki *et al.*, 1981). The observed Doppler velocities decrease to 200–250 m/s at ranges beyond 585 km. Figure 10a suggest that these echoes come from the F region.

In Fig. 10b (beam 15) the E region echoes come from ranges of 450–700 km and the echoes beyond 500 km are contaminated with the F region echoes. In our observations a maximum velocity of about 300 m/s on beam 15 appears at ranges of 450–500 km that corresponds to the 100–110 km altitudes in Fig. 10b. This suggests that the wave refraction in the E region is unnecessary or a little if any: if the refraction were effective, the ranges where the maximum velocity appears would be larger than 500 km (say, around 550 km). Again keep in mind that the importance/unimportance of the refraction is dependent on local time (see Figs. 8 and 9) and ionospheric conditions. The observed Doppler velocities decrease to 270–300 m/s at ranges beyond 700 km that correspond to the upper E and F region altitudes.

Another way to explain the observed range profiles relies on eqs. (1) and (2) telling that V_{ph} depends only on α when the irregularities are assumed to exist at around 110 km altitude. V_{ph} has a maximum of V_d at $\alpha = 0^\circ$ and rapidly decreases with increasing α .

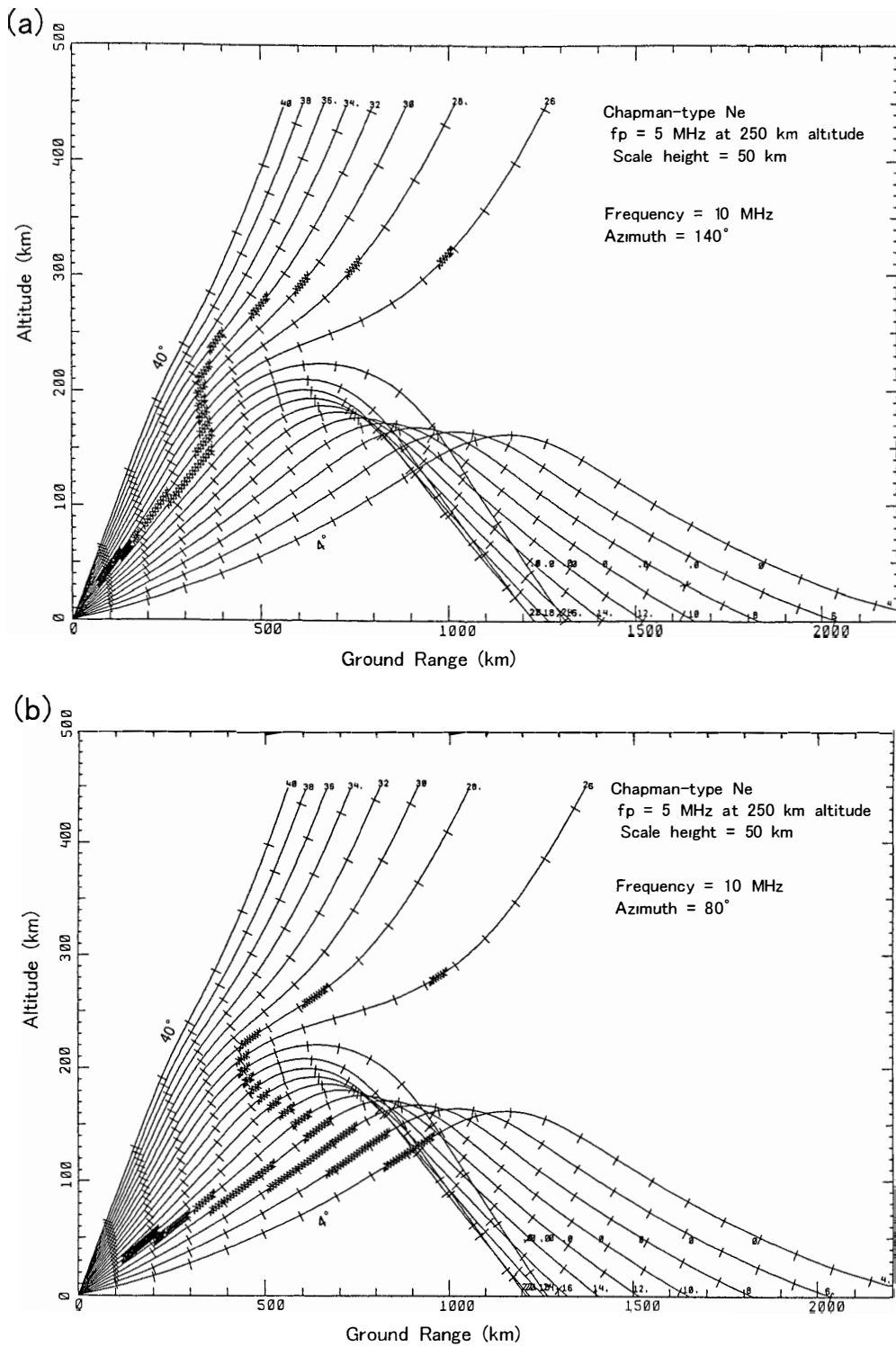


Fig. 10. Ray-tracings for 10 MHz wave emitted from Syowa with elevation angles of 4° – 40° (2° step) at azimuths of (a) 140° and (b) 80° . Positions where ray paths are nearly perpendicular (between 89° and 91°) to the geomagnetic field are indicated by the crosses. Slant ranges (100 km step) from Syowa are marked. A Chapman-type ionospheric electron density distribution (plasma frequency = 5 MHz at an altitude of 250 km, scale height = 50 km) is assumed for the calculations.

Ogawa *et al.* (1980, 1982) found that this “aspect angle dependence” of V_{ph} explains well statistical velocity profiles obtained with a VHF (50 MHz) auroral radar at Siple Station, Antarctica. The velocity in Fig. 6b has a maximum at a range of 450 km where $\alpha \simeq 0^\circ$ and decreases with increasing and decreasing range, that is, with increasing α (see Fig. 1). Thus, it is possible to explain the velocity variations between 300 and 700 km by the α dependence for the 110 km altitude echoes. Similar explanation is valid for the profiles in Fig. 6a when the wave refraction, which replaces the maximum velocity range from 280 km to 400 km, is taken into account.

When explaining the range profiles of Doppler velocity, we must also consider the fact that electric fields in the auroral zone usually increase toward the pole (*e.g.*, Ogawa *et al.*, 1982; Heppner and Maynard, 1987). Such signatures are discernible in some range profiles shown in Figs. 6–9.

The standard deviations shown in Figs. 6–9 indicate that the observed Doppler velocities at ranges beyond 300–350 km are between ~ 0 and 600 m/s. This velocity extent is caused by the type-1 (two-stream) and type-2 (gradient-drift) irregularities in the *E* region. At farther ranges beyond, say, 700 km, the velocities can be related to the current-convective and gradient-drift instabilities in the *F* region. When no wave refraction is considered, the altitude resolution corresponding to a range resolution of 45 km becomes poorer with increasing elevation angle of ray path; for example, 4, 8, 15, and 23 km for 5° , 10° , 20° , and 30° , respectively. When the elevation angle is larger than 20° , the altitude resolution exceeds the thickness of the electrojet (~ 15 km), which means that the observed Doppler velocities do not well represent the altitude profile of plasma velocity in the electrojet, but rather gives a velocity averaged over the thickness of the electrojet. This may be the reason why the observed Doppler velocities in the *E* region are below 500 m/s (Fig. 6). When the wave refraction capable of refracting waves downward is effective, the altitude resolutions may become better than the values described above. Anyway, to investigate the velocity structures in the *E* region, we need observations using range (~ 15 km) and time (≤ 1 min) resolutions higher than the present cases. See a paper by Uspensky *et al.* (1994) for modeling of the *E* region radar echoes.

In this paper we have analyzed only the Doppler velocity data. Doppler spectral widths give also important information on the plasma instability processes in the *E* region. Simultaneous analysis of both mean Doppler velocity and spectral width is needed in the future.

5.2. Short-range echoes

Figure 6 indicates the existence of echoes (irregularities) at ranges of 180–270 km. Judging from Figs. 2 and 10, it is difficult to relate all of these echoes to the field-aligned irregularities at 100–120 km altitudes. Although the origins of these echoes are not clear at this stage, we discuss some possibilities to explain the short-range (low-altitude) echoes.

The new instability proposed by Dimant and Sudan (1995, 1997) seems to be attractive for the echoes below the *E* region (Section 2). This instability, however, needs high *E* exceeding 50 mV/m that is expected only near midnight under strongly disturbed conditions, that is, under *K*-indices beyond, say, 5. Such events were rare in

our case (see Fig. 4). Rather, Figs. 8 and 9 suggest the existence of the low-altitude echoes at all hours.

Our scheme for the data selection (Section 4.1) might not always function to exclude all meteor echoes from the original data base. Previous 50 MHz meteor radar observations at Syowa Station found meteor echo altitudes of 80–100 km with a peak at 90 km and echo ranges of 120–600 km (Ogawa *et al.*, 1985). Hourly variation of the number of meteor echoes showed a maximum at around 06 UT and a minimum at around 21 UT with a ratio of 5 to 1. From meteor echo observations using a SuperDARN radar, Hall *et al.* (1997) found a peak altitude of 94 ± 3 km and meteor echo ranges of 180–700 km. Thus, there is a possibility that our data base at altitudes of 80–110 km, in particular, at around 06 UT includes meteor echoes. Doppler velocities (\approx neutral wind velocities) derived from meteor echoes are less than ± 50 m/s (e.g., Tanaka *et al.*, 1988; Hall *et al.*, 1997) although these velocities may exceed ± 100 m/s under disturbed conditions. In Fig. 6, however, the mean velocities at ranges less than 270 km are about 100 m/s with standard deviations of 100 m/s, which suggests that echoes other than meteor echoes also contribute to the velocity profiles.

Plasma turbulence in the *D* and lower *E* regions can be excited through turbulent motion of the neutral atmosphere (Gurevich *et al.*, 1997). Schlegel and Gurevich (1997) applied Gurevich *et al.*'s theory to coherent backscatter experiments with radars having a frequency range of 5–150 MHz and found that the backscatter cross-section increases strongly with decreasing radar frequency and that the mean Doppler velocity is close to neutral wind motions (≤ 50 m/s). At a radar frequency of 10 MHz (our case), the echo altitudes were expected to be between 80 and 110 km. Kyzyurov (2000) has recently presented a new theory for the production of plasma irregularities (scale lengths of decameter-hectometer) in mid-latitude sporadic *E* layer due to the neutral atmosphere turbulence. At this stage we do not know whether these theories are applicable to our data or not because more theoretical development is needed.

Note that radar echoes due to the meteors and neutral turbulence do not always have geomagnetic aspect sensitivity. This means that these echoes may be also included in the Doppler velocity profiles at ranges beyond 270 km in Figs. 6–9.

6. Conclusions

Using a large number of Doppler velocity data from the Syowa East HF radar, we have obtained range profiles of mean and standard deviation of the Doppler velocity. *K*-indices at Syowa station during the observation period spanned from 0 to 7 with a maximum occurrence at $K=1$. Although the standard deviations are very large, the following results are obtained:

1) Mean Doppler velocity has a minimum of ~ 100 m/s at ranges of 180–225 km and maxima of 300 and 350 m/s at ranges of about 400 and 450–500 km for beam 0 and 15, respectively. It decreases to about 250 m/s at 600–700 km and then gradually increases with range. Signatures indicating poleward-increasing electric field are discernible in range profiles of Doppler velocity. Although we cannot determine exact altitudes of the echo regions because of a coarse spatial resolution of the radar (45 km) as well as radar wave refraction, almost all the echoes are believed to have been produced through

plasma instabilities in the ionosphere.

2) The small Doppler velocities (≤ 100 m/s) at short ranges (low altitudes) may be partly caused by neutral winds and/or turbulence of the neutral atmosphere. This possibility should be further investigated in the future.

3) Relying on that maximum phase velocities of plasma waves should appear near an altitude of 110 km, it is concluded that HF wave refraction due to enhanced *E* region electron density is operative for radar beams nearly perpendicular to *L*-shells. Because of this refraction effect, the maximum Doppler velocity appears at ranges of about 360 km in the morning and about 400 km in the afternoon. We suppose that the difference in range (40 km) was caused by a lowering of the enhanced density region in the morning sector.

Finally, the current operation method of the Syowa East radar is not always suitable for studying the physics of the *D* and *E* region irregularities. Higher spatial (~ 15 km) and time (≤ 1 min) resolutions are needed in the future study.

Acknowledgments

We thank all the staff who contributed to the HF radar observations at Syowa Station and M. Fukumoto for his partial support to data analysis. HF ray-tracing results were kindly supplied by A. Frey. This research is supported by the Grant-in Aid for Scientific Research (A: 11304029) from Japan Society for the Promotion of Science (JSPS). The Ministry of Education, Science, Sports and Culture (MONBUSHO) supports the the Syowa HF radar system.

The editor thanks Dr. S. Milan and another referee for their help in evaluating this paper.

References

- Blix, T.A., Thrane, E.V., Kirkwood, S., Dimant, Y.S. and Sudan, R.N. (1996): Experimental evidence for unstable waves in the lower *E*/upper *D*-region excited near bisector between the electric field and the drift velocity. *Geophys. Res. Lett.*, **23**, 2137–2140.
- Dimant, Y.S. and Sudan, R.N. (1995): Kinetic theory of the Farley-Buneman instability in the *E* region of the ionosphere. *J. Geophys. Res.*, **100**, 14605–14623.
- Dimant, Y.S. and Sudan, R.N. (1997): Physical nature of a new cross-field current-driven instability in the lower ionosphere. *J. Geophys. Res.*, **102**, 2551–2563.
- Fejer, B.G., Providakes, J. and Farley, D.T. (1984): Theory of plasma waves in the auroral *E* region. *J. Geophys. Res.*, **89**, 7487–7494.
- Fukumoto, M., Nishitani, N., Ogawa, T., Sato, N., Yamagishi, H. and Yukimatu, A.S. (1999): Statistical analysis of echo power, Doppler velocity and spectral width obtained with the Syowa South HF radar. *Adv. Polar Upper Atmos. Res.*, **13**, 37–47.
- Fukumoto, M., Nishitani, N., Ogawa, T., Sato, N., Yamagishi, H. and Yukimatu, A.S. (2000): Statistical study of Doppler velocity and echo power around 75° magnetic latitude using data obtained with the Syowa East HF radar in 1997. *Adv. Polar Upper Atmos. Res.*, **14**, 93–102.
- Greenwald, R.A., Baker, K.B., Dudeney, J.R., Pinnock, M., Jones, T.B., Thomas, E.C., Villain, J.-P., Cerisier, J.-C., Senior, C., Hanuise, C., Hunsucker, R.D., Sofko, G., Koehler, J., Nielsen, E., Pellinen, R., Walker, A.D. M., Sato, N. and Yamagishi, H. (1995): DARN/SuperDARN: A global view of the dynamics of high-latitude convection. *Space Sci. Rev.*, **71**, 761–796.
- Gurevich, A.V., Borisov, N.D. and Zybin, K.P. (1997): Ionospheric turbulence induced in the lower part of the *E* region by the turbulence of the neutral atmosphere. *J. Geophys. Res.*, **102**, 379–388.

- Haldoupis, C. (1989): A review of radio studies of auroral *E* region ionospheric irregularities. *Ann. Geophys.*, **7**, 239–258.
- Hall, G.E., MacDougall, J.W., Moorcroft, D.R., St.-Maurice, J.-P., Manson, A.H. and Meek, C.E. (1997): Super Dual Auroral Radar Network observations of meteor echoes. *J. Geophys. Res.*, **102**, 14603–14614.
- Hanuse, C., Villain, J.P., Cerisier, J.C., Senior, C., Ruohoniemi, J.M., Greenwald, R. A. and Baker, K.B. (1991): Statistical study of high-latitude E-region Doppler spectra obtained with the SHERPA HF radar. *Ann. Geophys.*, **9**, 273–285.
- Hardy, D.A., Gussenhoven, M.S. and Holeman, E. (1985): A statistical model of auroral precipitation. *J. Geophys. Res.*, **90**, 4229–4248.
- Heppner, J.P. and Maynard, N.C. (1987): Empirical high-latitude electric field models. *J. Geophys. Res.*, **92**, 4467–4489.
- Kagan, L.M. and Kelley, M.C. (1998): A wind-driven gradient drift mechanism for mid-latitude *E*-region ionospheric irregularities. *Geophys. Res. Lett.*, **25**, 4141–4144.
- Kagan, L.M. and Kelley, M.C. (2000): A thermal mechanism for generation of small-scale irregularities in the ionospheric E region. *J. Geophys. Res.*, **105**, 5291–5303.
- Kagan, L.M., Ogawa, T., Fukao, S. and Yamamoto, M. (2000): A role of neutral motions in formation of midlatitude *E*-region field-aligned irregularities. *Geophys. Res. Lett.*, **27**, 939–942.
- Kamide, Y. and Brekke, A. (1977): Altitude of the eastward and westward auroral electrojets. *J. Geophys. Res.*, **82**, 2851–2853.
- Koustov, A.V., Igarashi, K., André D., Ohtaka, K., Sato, N., Yamagishi, H. and Yukimatu, A.S. (2001): Observations of 50- and 12-MHz auroral coherent echoes at the Antarctic Syowa Station. *J. Geophys. Res.*, **106**, 12875–12887.
- Kozyurov, Yu.V. (2000): On the spectrum of mid-latitude sporadic-*E* irregularities. *Ann. Geophys.*, **18**, 1283–1292.
- Makarevitch, R.A., Ogawa, T., Igarashi, K., Koustov, A.V., Sato, N., Yamagishi, H. and Yukimatu, A.S. (2001): On the power-velocity relationship for 12- and 50-MHz auroral coherent echoes. *J. Geophys. Res.*, **106**, 15455–15469.
- Milan, S.E. and Lester, M. (1998): Simultaneous observations at different altitudes of ionospheric backscatter in the eastward electrojet. *Ann. Geophys.*, **16**, 55–68.
- Milan, S.E., Yeoman, T.K., Lester, M., Thomas, E.C. and Jones, T.B. (1997): Initial backscatter occurrence statistics from the CUTLASS HF radars. *Ann. Geophys.*, **15**, 703–718.
- Miyazaki, S., Ogawa, T. and Mori, H. (1981): Some features of nighttime *D* and *E* region electron density profiles in the polar ionosphere. *Mem. Natl Inst. Polar Res., Spec. Issue*, **18**, 304–311.
- Ogawa, T. (1996): Radar observations of ionospheric irregularities at Syowa Station, Antarctica: A brief overview. *Ann. Geophys.*, **14**, 1454–1461.
- Ogawa, T. and Igarashi, K. (1982): VHF radar observation of auroral *E*-region irregularities associated with moving-arcs. *Mem. Natl Inst. Polar Res., Spec. Issue*, **22**, 125–139.
- Ogawa, T., Mori, H. and Miyazaki, S. (1976): Rocket observations of electron density irregularities in the Antarctic auroral *E* region. *J. Geophys. Res.*, **81**, 4013–4015.
- Ogawa, T., Balsley, B.B., Ecklund, W.L., Carter, D.A. and Johnston, P.E. (1980): Aspect angle dependence of irregularity phase velocities in the auroral electrojet. *Geophys. Res. Lett.*, **7**, 1081–1084.
- Ogawa, T., Balsley, B.B., Ecklund, W.L., Carter, D.A. and Johnston, P.E. (1982): Auroral radar observations at Siple Station, Antarctica. *J. Atmos. Terr. Phys.*, **44**, 529–537.
- Ogawa, T., Igarashi, K., Kuratani, Y., Fujii, R. and Hirasawa, T. (1985): Some initial results of 50 MHz meteor radar observation at Syowa Station. *Mem. Natl Inst. Polar Res., Spec. Issue*, **36**, 254–263.
- Ogawa, T., Yamagishi, H., Ayukawa, I., Tanaka, T. and Igarashi, K. (1989): Simultaneous observations of radar aurora and visible aurora over Mizuho Station. *Proc. NIPR Symp. Upper Atmos. Phys.*, **2**, 103–109.
- Ogawa, T., Hirasawa, T., Ejiri, M., Sato, N., Yamagishi, H., Fujii, R. and Igarashi, K. (1990): HF radar experiment at Syowa Station for the study of high-latitude ionosphere-2: A capability. *Proc. NIPR Symp. Upper Atmos. Phys.*, **3**, 91–95.
- Ogawa, T., Yamamoto, M. and Fukao, S. (1995): Middle and upper atmosphere radar observations of turbulence and movement of midlatitude sporadic *E* irregularities. *J. Geophys. Res.*, **100**, 12173–

12188.

- Ossakow, S.L. and Chaturvedi, P.K. (1979): Current convective instability in the diffuse aurora. *Geophys. Res. Lett.*, **6**, 332–334.
- Ruohoniemi, J.M., Greenwald, R.A., Baker, K.B., Villain, J.P. and McCready, M.A. (1987): Drift motions of small-scale irregularities in the high-latitude *F* region: An experimental comparison with plasma drift motions. *J. Geophys. Res.*, **92**, 4553–4564.
- Schlegel, K. and Gurevich, A.V. (1997): Radar backscatter from plasma irregularities of the lower E region induced by neutral turbulence. *Ann. Geophys.*, **15**, 870–877.
- Takeuchi, S., Ookawa, T., Setoguchi, T., Ozeki, J., Kikuchi, M., Kadokura, A. and Taguchi, M. (1999): Upper atmosphere physics data obtained at Syowa Station. *JARE Data Rep.*, **243** (Upper Atmos. Phys. 17), 204 p.
- Tanaka, T., Ogawa, T. and Nomura, A. (1988): Neutral wind observations by 50 MHz meteor radar at Syowa Station. *Proc. NIPR Symp. Upper Atmos. Phys.*, **1**, 84–87.
- Tsunoda, R.T. (1988): High-latitude *F* region irregularities: A review and synthesis. *Rev. Geophys.*, **26**, 719–760.
- Tsunoda, R.T., Olesen, J.K. and Stauning, P. (1997): Radar evidence for a new low-frequency crossed-field plasma instability in the polar mesopause region: A case study. *Geophys. Res. Lett.*, **24**, 1215–1218.
- Uspensky, M.V., Kustov, A.V., Sofko, J.G., Koehler, J.A., Villain, J.P., Hanuise, C., Ruohoniemi, J.M. and Williams, P.J. (1994): Ionospheric refraction effects in slant range profiles of auroral HF coherent echoes. *Radio Sci.*, **29**, 503–517.
- Villain, J.P., Greenwald, R. and Vickery, J.F. (1984): HF ray tracing at high latitudes using measured meridional electron density distributions. *Radio Sci.*, **19**, 359–374.
- Yamamoto, M., Fuako, S., Woodman, R.F., Ogawa, T., Tsuda, T. and Kato, S. (1991): Midlatitude *E*-region field-aligned irregularities observed with the MU radar. *J. Geophys. Res.*, **96**, 15943–15949.

(Received January 11, 2001; Revised manuscript accepted June 6, 2001)